Impact of perceptual learning on resting-state fMRI connectivity: A supervised classification study

Mehdi Rahim
CEA/SHFJ & INRIA/CEA Parietal
4 place du général Leclerc
91401 Orsay, cedex FRANCE
Email: rahim.mehdi@gmail.com

Philippe Ciuciu, Salma Bougacha
CEA/NeuroSpin & INRIA/CEA Parietal
CEA Saclay - Bât 145
91191 Gif-sur-Yvette, cedex FRANCE
Emails: philippe.ciuciu@cea.fr, salmabougacha@hotmail.com

***Abstract*—Perceptual learning sculpts ongoing brain activity [1]. This finding has been observed by statistically comparing the functional connectivity (FC) patterns computed from resting-state functional MRI (rs-fMRI) data recorded before and after intensive training to a visual attention task. Hence, functional connectivity serves a dynamic role in brain function, supporting the consolidation of previous experience. Following this line of research, we trained three groups of individuals to a visual discrimination task during a magneto-encephalography (MEG) experiment [2]. The same individuals were then scanned in rs-fMRI. Here, in a supervised classification framework, we demonstrate that FC metrics computed on rs-fMRI data are able to predict the type of training the participants received. On top of that, we show that the prediction accuracies based on tangent embedding FC measure outperform those based on our recently developed multivariate wavelet-based Hurst exponent estimator [3], which captures low frequency fluctuations in ongoing brain activity too.**

I. Introduction

Multisensory interactions are ubiquitous in cortex and sensory cortices may be supramodal ie, capable of functional selectivity irrespective of the sensory modality of inputs [4], [5]. In [2], we asked whether learning to discriminate visual coherence could benefit from supramodal processing. To this end, three groups of twelve participants were briefly trained to discriminate which of a red or green intermixed population of random-dot-kinematograms (RDKs) was most coherent in a visual display while being recorded with MEG (see Fig. 1). During training, participants heard no sound (**V**), congruent acoustic textures (**AV**) or auditory noise (**AVn**); importantly, congruent acoustic textures shared the temporal statistics – i.e. coherence – of visual RDKs. After training, the AV group significantly outperformed participants trained in V and AVn although they were not aware of their progress. In pre- and post-training blocks, all participants were tested without sound and with the same set of RDKs.

After the MEG experiment, the same individuals underwent a rs-fMRI scanning session of about 9 min to determine whether multi-perceptual learning impacted intrinsic brain activity and functional networks. These data allow us to investigate functional connectivity (FC) analysis. In contrast to [1], we could not contrast FC metrics before and after learning since no fMRI data were collected before. Instead, in this paper we focus on discriminating the three groups relying solely on FC metrics extracted after the learning process. Such a discrimination proves that multi-perceptual learning shapes ongoing brain activity in a different manner than purely visual one and hence confirms to some extent previous findings [1].

The paper is organized as follows. In Sec. II, we describe our learning MEG experiment [2]. In Sec. III, the proposed FC analysis pipeline is presented. Group-level results are reported in Sec. IV together with the prediction accuracies of supervised classifiers that perform binary classification (eg, **AV-V**) from FC measures as input features. Also, our results are compared in terms of classification performance with those recently derived on the same dataset from wavelet-based Hurst exponent estimates [3]. Conclusions are drawn in Section V.

II. Brain networks definition from MEG data

Fig. 2(top) provides an illustration of regions of interest (ROIs) in the sensor and source space showing significant post-training changes in neural responses after training in the **V**, **AV** and **AVn** groups. Significant changes in hMT+, V4, ITC and vlPFC were common to all groups whereas pSTS, mSTS, and AC were specific to the multisensory **AV** and **AVn** groups. As shown in Fig. 2(bottom), the network observed in post-multisensory training was more extensive than in purely visual training. Strikingly, the pattern of activation in both **AVn** and **AV** was notably reversed in several regions including pSTS, AC, mSTS and V4: this suggests selective modulations of these cortical regions based on the stimuli presented during training but also direct functional connectivity between these regions. No significant changes of activity were observed in these regions for the **V** group.

Common to all groups, hMT+ (supramodal coherence selectivity) and vlPFC (selective attention) showed discriminative cortical responses as a function of the learned coherence levels. Additionally, all groups showed an increased activity in ITC only for the easy coherence levels suggesting an improvement in color-motion binding. In hMT+, the increase spread of neural response was shared by **V** and **AVn**, whereas selective activity was seen for **AV** solely.

Furthermore, solely for **AV**, activity in multisensory cortices (mSTS, pSTS) correlated with post-training performances (see [2] for details); additionally, the latencies of these effects suggested feedback from vlPFC to hMT+ possibly

978-0-9928-6265-7/16/$31.00 ©2016 IEEE

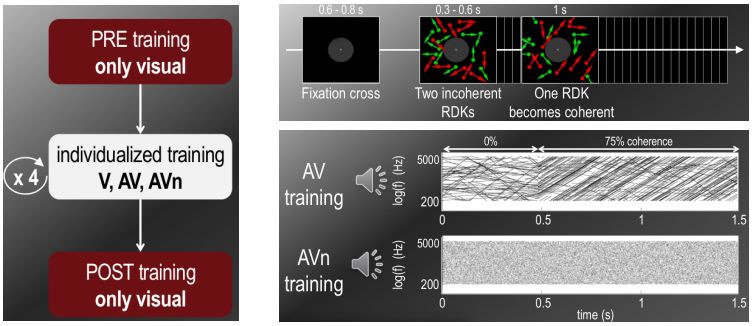

Fig. 1. Multi-perceptual learning experiment undertaken during MEG acquisition (90 min). **Left**: Pre- and post-training task blocks consisting of visual stimuli depicted on top-right. Three different groups of individuals performed either visual (**V**), congruent auditory and visual (**AV**) or incongruent auditory and visual (**AVn**) training. **Top right**: Two random dot kinematograms (green and red) were presented to the individual. First, they moved incoherently during a period ranging from 0.3 s to 0.6 s. Then, one population of dots starts moving coherently for 1 s. Next, the participant must press a button to decide whether the coherent dots population is red or green. The task difficulty was varied by changing the proportion of dots moving in the same direction (easy level: 95 %, very difficult level: 15 %). **Bottom right**: Acoustic stimuli delivered to individuals in the **AV** and **AVn** groups. In **AV**, an acoustic texture was designed to map the direction of coherent dots point-by-point. In **AVn**, only white noise was mapped point-wise to dots.

mediated by temporal cortices in **AV** and **AVn**. Altogether, we interpret our results in the context of the Reverse Hierarchy Theory (RHT) of learning [6] in which supramodal processing optimizes visual perceptual learning by capitalizing on sensory-invariant representations, here, global coherence levels across sensory modalities.

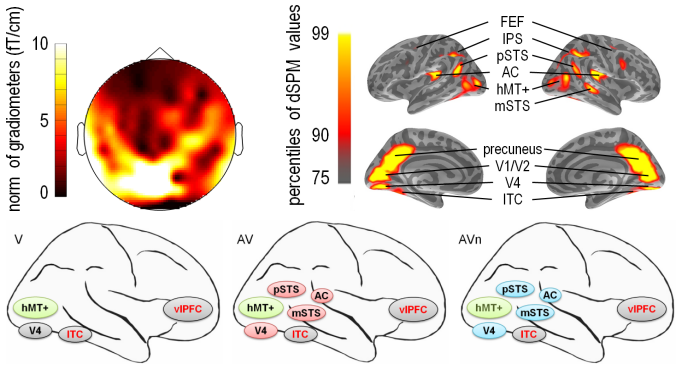

Fig. 2. **Top-left**: Topography of ERF obtained in response to the presentation of incoherent visual RDKs is provided for the norm of gradiometers averaged over 100 to 300 ms post-incoherence onset ($n = 36$ subjects). **Top-right**: The corresponding current source estimates (MNE, dSPM) are provided. The extent of a given label or ROI in source space was defined by thresholding the dSPM estimates at the 90th percentile of all dSPM values. FEF: Frontal Eye Field. IPS: Inferior Parietal Sulcus. pSTS: posterior Superior Temporal Sulcus. AC: Auditory Cortex. mSTS: middle Superior Temporal Sulcus. ITC: Inferior Temporal Cortex. **Bottom**: ROIs where activity is specifically increased (red) or decreased (blue) in each group. Common changes are depicted in gray.

III. Functional Connectivity Analysis

Whole brain fMRI BOLD data were collected on 36 individuals on a 3.0 Tesla Siemens Tim Trio scanner using a gradient-echo EPI sequence. Scans were acquired at every TR $= 1.05$ s using the following parameters (TE $= 30$ ms, matrix size: 64×64, FOV=192×192 mm^2, slice-thickness=6 mm). A single run of $N = 514$ scans of rs-fMRI was collected in each individual. The general pipeline we implemented for FC analysis of rs-fMRI data is depicted in Fig. 3. Hereafter, we summarize the most important aspects of each step.

A. Definition of Regions of interest

Regarding the ROI definition, we investigated two different strategies. The first set of ROIs was informed by MEG data and consisted of extracting 22 regions (11 in each hemisphere, see Fig. 2 for the 20 ROIs on top of which we added the vlPFC bilaterally) involved during perceptual learning in each individual. Once identified in each individual, we extracted the coordinates of these regions in the MNI space owing to spatial normalization of anatomical MRI (aMRI) data and co-registration of MEG data with the individual's aMRI. Next, spheres of 6-mm radius were defined around the centres given by the above-mentioned coordinates to extract fMRI signals.

The second strategy relied on more brain regions using the multi-subject dictionary learning (MSDL) atlas. It has been designed over the last years in our group [7]. It has 39 ROIs grouped in several resting-state networks that cover the whole brain. It is available in `https://team.inria.fr/parietal/research`.

B. Preprocessing steps

As detailed in Fig. 3, fMRI time series were spatially preprocessed using a standard procedure: given the short TR value, slice timing correction was not applied. Instead, the scans were realigned for motion correction. Coregistration with anatomy was performed to ensure good match between anatomical and functional data. Spatial normalization was performed using the DARTEL toolbox. Last, spatial smoothing was applied to each volume using an isotropic Gaussian kernel with FWHM $= 6$ mm.

The presence of noise in fMRI signals and the absence of any experimental paradigm in resting-state recordings calls for an accurate control of putative bias which results in misleading connectivity between unrelated regions. To face this concern

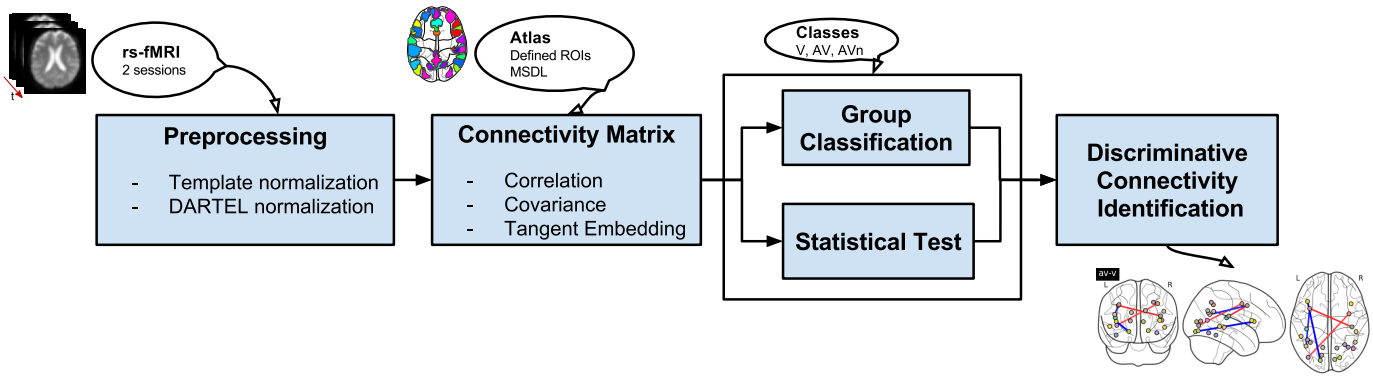

Fig. 3. Proposed pipeline for analyzing rs-fMRI data from pre-processings (temporal and spatial including normalization using DARTEL in SPM12) to supervised classification (binary group comparisons like **AV-V**). The outcome of supervised classification allows us to unravel the discriminant functional interactions between groups. This pipeline was implemented in `Python` language using the `nipype` interface and the nilearn software (`http://nilearn.github.io/`).

and improve results consistency, one needs to appropriately characterize and remove noise effects. Here, we defined a general linear model to regress out confounds accounting for head motion (3 translation and 3 rotation parameters per frame) and their derivatives as well as a linear detrending regressor to remove the global drift due to physiological and thermal noises. Finally, the time series within each ROI was band-pass filtered between 0.01 Hz and 0.1 Hz to reduce the effect of the low frequency drift and the high frequency noise.

C. Functional connectivity metrics

We investigated the use of four different connectivity metrics to probe functional interactions between ROIs from rs-fMRI data: Pearson correlation, sparse graph lasso, sparse group-covariance matrix and tangent embedding. Hereafter, we summarize these four estimators. We report the results we got using tangent embedding since this technique was the most accurate in terms of classification performance.

Consider regions i and j and denote by ρ the Pearson correlation coefficient, then $\rho = \frac{\boldsymbol{C}_{i,j}}{\sqrt{\boldsymbol{C}_{i,i}}\sqrt{\boldsymbol{C}_{j,j}}}$ where covariance matrix $\boldsymbol{C}$ is known to be well approximated with the classical maximum likelihood estimator (MLE or "empirical covariance" ie $\frac{1}{N}\boldsymbol{X}^T\boldsymbol{X}$ if $\boldsymbol{X}^{N\times p}$ denotes the timeseries across p ROIs), provided the number of observations (here N, the number of scans) is large enough as compared to the number of features (here p, the number of voxels or ROIs). In this study when focusing on 22 ROIs only ($p \ll N$), the MLE can be a good estimator of the eigenvalues of the covariance matrix, and the precision matrix obtained from its inversion ($\boldsymbol{K} = \boldsymbol{C}^{-1}$) may be accurate enough. However, when considering the MSDL atlas p and N are of the same order of magnitude, hence $N < p(p+1)/2$ and the performance of the covariance MLE degrades. To avoid such inversion problem, one usually resorts to the regularization of the precision matrix. The latter is proportional to the partial correlation matrix which gives partial independence relationship. Hence, if two features are independent conditionally on the others, the corresponding coefficient in the precision matrix will be zero. This is why it makes sense to estimate a sparse precision matrix: by learning independence relations from the data, the estimation of the covariance matrix is better conditioned. As a consequence, we tested the *Graph-lasso* estimator that uses an ℓ_1 penalty to enforce sparsity on the precision matrix: the higher its α parameter, the sparser the precision matrix $\boldsymbol{K}$ is:

$$\hat{\boldsymbol{K}} = \operatorname{argmin}_{\boldsymbol{K}} \left(\operatorname{tr} \boldsymbol{C}\boldsymbol{K} - \log\det \boldsymbol{K} + \alpha \|\boldsymbol{K}\|_1 \right) \quad (1)$$

where $\|\boldsymbol{K}\|_1$ is the sum of the absolute values of off-diagonal coefficients of $\boldsymbol{K}$. The algorithm employed to solve this problem is the Graph-lasso algorithm proposed in [8].

We also tested the group-sparse covariance estimator which consists of imposing the same structure of conditional independence across subjects ie, the zeros in the different precision matrices should be at the same positions. This was proposed in [9] as a group-level extension of Graph-Lasso (1) by penalizing precision matrices using a mixed norm.

Another possible construction of group covariance matrix relies on the principle of maximum entropy, assuming that the individual covariance matrices $(\boldsymbol{C}_s)_{s=1}^n$ derive from a generalized matrix-valued Gaussian distribution [10] with mean covariance matrix $\boldsymbol{C}^*$. The discrepancy of each $\boldsymbol{C}_s$ from $\boldsymbol{C}^*$ is measured by embedding the tangent space to the set of non-singular covariances into symmetric matrices [11]:

$$\forall s = 1, \cdots n: \quad \operatorname{Log}(\boldsymbol{C}^{*-\frac{1}{2}} \boldsymbol{C}_s \boldsymbol{C}^{*-\frac{1}{2}}) \quad (2)$$

where Log denotes the matrix logarithm. Upper triangular coefficients of this discrepancy matrix are connectivity features.

D. Scale-free brain dynamics as alternative descriptors

In a previous work [3], we measured Hurst exponents on the same rs-fMRI dataset to assess the modulation of scale-free ($1/f$ power spectrum) brain dynamics induced by perceptual learning. To this end, we used a univariate wavelet-based estimator to fit the linear slope on the wavelet-based power spectrum within the $(0.01 - 0.1)$ Hz range [12]. Technically, we used Daubechies wavelets with 2 vanishing moments. We already demonstrated that these exponents are relevant

features for classifying the type of training underwent by the participants.

E. Connectivity-based classification

We used the logistic regression classifier to predict binary outcomes and to compare each group pair such as (**AV-V**). Input features are functional connectivity matrices (lower triangular part of covariance matrix: $p(p-1)/2$ components per participant), yielding a feature matrix $\mathbf{F} = (\mathbf{f}_1^T, ..., \mathbf{f}_n^T)^T$ of dimension $(n, p(p-1)/2)$. Logistic regression is a linear model where the weight vector $\mathbf{w}$ is estimated to fit the features $\mathbf{F}$ to the participants group $\mathbf{y} = (y_1, ..., y_n)^T \in \{0,1\}^n$ as:

$$\widehat{\mathbf{w}} = \underset{\mathbf{w}\in\mathbb{R}^{p(p-1)/2},\, c\in\mathbb{R}}{\operatorname{argmin}} \frac{\lambda}{2}\|\mathbf{w}\|_2^2 + \sum_{s=1}^{n} \log(e^{-y_s(\mathbf{f}_s\mathbf{w}+c)} + 1),$$

where λ controls the regularization, c is the intercept, and $\hat{\mathbf{w}}$ are the estimated connectivity model coefficients to define the specific group of a given participant s. High values in $\widehat{\mathbf{w}}$ can be interpreted as discriminative connectivity components between groups.

In our experiments, functional connectivity metrics were computed on the *whole* dataset. Then, each group pair of 24 individuals (taken out of 36) was split in training and test sets. The training set was composed of subjects randomly chosen in both groups with the same occurrence proportions. The classifier was assessed by a cross-validation scheme: A stratified-shuffle split loop with 100 iterations and a test fold size of 25% of the whole dataset. Our implementation was based on the `scikit-learn` package.

IV. Results

We applied the different sparse inverse covariance estimators to the 3 different groups of rs-fMRI data. In what follows, we report the best results we obtained with respect to our classification target, namely those derived from tangent embedding FC metrics (2) and the set of MEG-informed ROIs.

A. Within-group FC patterns

Statistical significant FC patterns are depicted in Fig. 4 for each group. Globally, one can notice that only positive interactions are retrieved in **V** whereas the converse finding is observed in **AVn**. A combination of positive and negative interactions is retrieved in **AV**. Importantly, left vlPFC is positively connected to V4 and hMT+ in **V** and **AV**, respectively. This confirms the particular role played by hMT+ in **AV** training. We did not report such involvement in other groups. Surprisingly, we observed significant negative interactions between AC and V1/V2 in **AV** in the left hemisphere whereas positive interaction is significantly recovered in **V**. This result may seem inconsistent with our previous observation in MEG (see Fig. 2) even though we have not performed FC analysis from MEG data so far. As first outlined in MEG, here from rs-fMRI data we also consistently observed the specific involvement of pSTS, mSTS and ITC through negative interactions with other regions in **AV** and **AVn**.

TABLE I
MEANS AND STANDARD DEVIATIONS OF PREDICTION ACCURACY (IN %) OF **AV-V** CLASSIFICATION ON TEST SETS ACROSS FOLDS.

	Tangent embed.	Correlation	Group sparse cov.
MSDL	82.0 ± 15.9	63.0 ± 17.1	61.7 ± 19.8
ROIs	**86.0 ± 12.6**	60.0 ± 18.3	72.3 ± 15.1

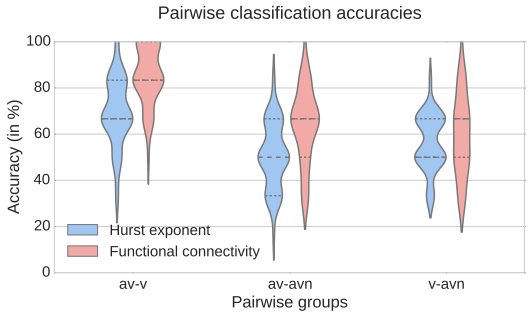

Fig. 5. Classification performances on functional connectivity measures (based on tangent space estimator) and wavelet-based Hurst exponents as input features to discriminate pairwise groups (**AV-V**, **AV-AVn** and **V-AVn**). Median is depicted in dashed line, quartiles in dotted lines.

B. Between-group comparisons

Instead of reporting two-sample t-test for group comparison, we performed supervised classification to predict the type of training the individuals received from their FC features. In addition to the prediction accuracy, the logistic regression model permits to highlight between-group functional connectivity differences that are statistically significant.

Table I summarizes the results we got for **AV-V** comparison using different connectivity metrics and atlases (see Fig. 3). It illustrates that the optimal combination is achieved by using the selected ROIs as atlas and the tangent embedding as a connectivity metric. Fig. 5 shows the prediction accuracies[1] for the 3 pairwise group comparisons, either by tangent embedding metric and wavelet-based Hurst exponent estimates computed over the same frequency range (0.01-0.1 Hz), see [3] for details. We observed similar trends: the AV training type is easier to discriminate from others. Interestingly, prediction accuracies based on FC features are improved by more than 15 % for every group comparison as compared to those relying on Hurst exponent estimates.

Beyond such improvements in terms of classification performance, statistically discriminative weights between **V** and **AV** in the logistic regression model are shown in Fig. 6. For ease of visualization, we provide both matrix and connectome views, the latter being a thresholded version of the former. When focusing on the connectome view, we observed that positive interactions are inter-hemispheric whereas negative ones are stick to the left hemisphere. Strikingly, the bilateral FEFs seem to bring the most salient FC differences between **V** and **AV**. Indeed, stronger interaction (in red) between hMT+ and FEF in **AV** might corroborate the selective increase of

[1]Box plots show the median and quartiles over 100 stratifications.

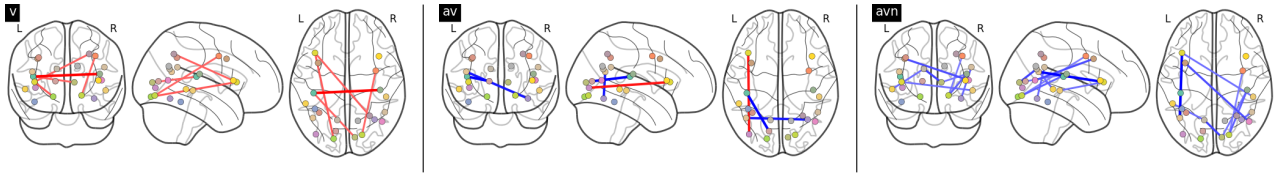

Fig. 4. Statistical significant functional interactions (positive and negative values are color coded in red and blue, respectively) within each group of individuals (**V**, **AV** and **AVn** from top to bottom), Bonferroni-corrected for multiple comparisons at $\alpha = 0.05$.

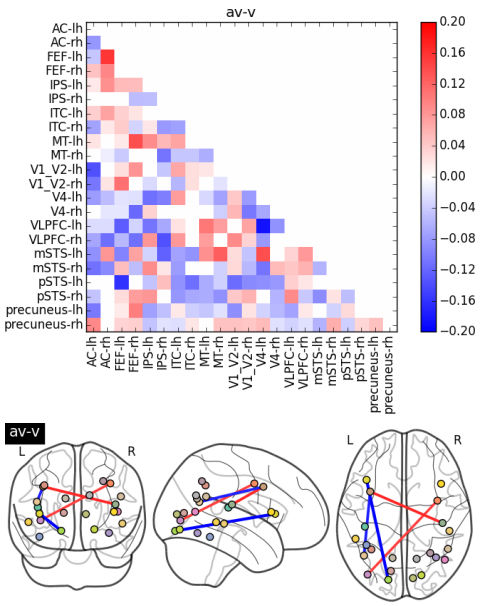

Fig. 6. Significant connectivity-based discriminative weights for the AV-V classification task. Positive/negative (red/blue) connections quantify between-group differences. Respectively, higher/lower connectivity in **AV** than **V**. **Top:** Matrix view with positive/negative weights. **Bottom**: Connectome view where only the most salient pairwise interactions are displayed. We observe that hMT+ is coded as MT. lh/rh stand for left and right hemispheres.

activity in hMT+ we observed on MEG data for this group. Also, larger covariation (in red) between FEF and AC in **AV** might reflect some binding mechanism between visual and auditory modalities that was trained in **AV** and not in **V**. The lower covariation (in blue) we found between V4 (color-form selectivity) and vlPFC (selective attention) in **AV** is compatible with the RHT since the individuals who performed purely visual training strengthened their connections between visual sensory inputs and decision-making areas. On the other hand, in the matrix view one can check that individuals in **AV** strengthened their connectivity betwen hMT+ (supramodal coherence selectivity) and vlPFC, which is a specificity of supramodal learning.

V. Conclusion

In this paper, we developed a functional connectivity analysis pipeline for rs-fMRI data that embeds different spatial/temporal preprocessings, different ROI definitions, complementary metrics for measuring interactions between regions and finally supervised classifiers. We assessed this pipeline on a MEG/fMRI dataset composed of 36 individuals who learned a visual discrimination task using either uni- or multi-perceptual training. We demonstrated that the prediction accuracy of auditory-visual training was reached with a rate of about 83 % as compared to purely visual training. This clearly outperforms our recent study [3] using Hurst exponents as input features to the classifier. Our results were achieved by optimally combining some specific pre-processings (DARTEL normalization, ...), the definition of MEG-informed ROIs and use of tangent-embedding FC metrics and logistic regression. They suggest the investigation of optimal combination of scale-free brain dynamics with pairwise interactions as proposed in the fractal connectivity model [13].

Acknowledgments

The authors warmly thank Régine Bricquet, Alexandre Abraham, and our team leader Bertrand Thirion for organizing the 2015 Parietal retreat, during which this project started.

References

[1] C. M. Lewis, A. Baldassarre, G. Committeri, G. L. Romani, and M. Corbetta, "Learning sculpts the spontaneous activity of the resting human brain," *pnas*, vol. 106, no. 41, pp. 17 558–17 563, 2009.
[2] N. Zilber, P. Ciuciu, A. Gramfort, and V. van Wassenhove, "Supramodal processing optimizes visual perceptual learning and plasticity," *Neuroimage*, vol. 93 Pt 1, pp. 32–46, 2014.
[3] H. Pellé, P. Ciuciu, M. Rahim, E. Dohmatob, P. Abry, and V. van Wassenhove, "Multivariate Hurst exponent estimation in fMRI. Application to brain decoding of perceptual learning," in *13th IEEE ISBI conference*, Prague, Czech Republic, Apr. 2016.
[4] A. Pascual-Leone and R. Hamilton, "The metamodal organization of the brain," *Prog. Brain Res.*, vol. 134, pp. 427–445, 2001.
[5] L. Renier, V. A. De, and J. Rauschecker, "Cortical plasticity and preserved function in early blindness," *Neurosci. Biobehav. Rev.*, vol. 134, pp. 1–11, 2013.
[6] M. Ahissar and S. Hochstein, "The reverse hierarchy theory of visual perceptual learning," *Trends Cogn. Sci.*, vol. 8, pp. 457–464, 2004.
[7] G. Varoquaux, A. Gramfort, F. Pedregosa, V. Michel, and B. Thirion, "Multi-subject dictionary learning to segment an atlas of brain spontaneous activity," in *Information Processing in Medical Imaging*, ser. Lecture Note in Computer Science. Springer, 2011, pp. 562–573.
[8] J. Friedman, T. Hastie, and R. Tibshirani, "Sparse inverse covariance estimation with the graphical lasso," *Biostatistics*, vol. 9, no. 3, 2008.
[9] G. Varoquaux, A. Gramfort, J.-B. Poline, and B. Thirion, "Brain covariance selection: better individual functional connectivity models using population prior," in *NIPS*, 2010, pp. 2334–2342.
[10] X. Pennec, P. Fillard, and N. Ayache, "A Riemannian framework for tensor computing," *Int J Comp Vision*, vol. 66, pp. 41–66, 2006.
[11] G. Varoquaux, F. Baronnet, A. Kleinschmidt, P. Fillard, and B. Thirion, "Detection of brain functional-connectivity difference in post-stroke patients using group-level covariance modeling," in *MICCAI*, 2010.
[12] D. Veitch and P. Abry, "A wavelet based joint estimator of the parameters of long-range dependence," *IEEE Transactions on Information Theory*, vol. 45, no. 3, pp. 878–897, 1999.
[13] P. Ciuciu, P. Abry, and B. J. He, "Interplay between functional connectivity and scale-free dynamics in intrinsic fMRI networks," *Neuroimage*, vol. 95, pp. 248–263, 2014.